Available online at www.sciencedirect.com
ScienceDirect
Journal of Power Sources 161 (2006) 743–752
JOURNAL OF POWER SOURCES
www.elsevier.com/locate/jpowsour

Electrocatalytic reduction of O_2 and H_2O_2 by adsorbed cobalt tetramethoxyphenyl porphyrin and its application for fuel cell cathodes

Hansan Liu [a], Lei Zhang [a], Jiujun Zhang [a,*], Dave Ghosh [a], Joey Jung [b,**], Bruce W. Downing [b], Earl Whittemore [b]

[a] *Institute for Fuel Cell Innovation, National Research Council of Canada, Vancouver, BC, Canada V6T 1W5*
[b] *R&D, MagPower Systems Inc., Delta, BC, Canada V4K 5B8*

Received 11 March 2006; received in revised form 28 April 2006; accepted 28 April 2006
Available online 14 June 2006

Abstract

In this paper, the mechanism and kinetics of oxygen and hydrogen peroxide electrochemical reduction that is catalyzed by an adsorbed cobalt tetramethoxyphenyl porphyrin (CoTMPP) on a graphite electrode were investigated using cyclic voltammetry (CV) and the rotating disk electrode (RDE) technique. The temperature and anion effects on O_2 and H_2O_2 electroreduction processes were also studied. The pH dependencies of cobalt redox centers, and oxygen and hydrogen peroxide reductions were measured for the purpose of exploring the reaction mechanism. In neutral solutions, the oxygen reduction reaction was observed to be a two-electron process, producing H_2O_2 in the low potential polarization range. In the high potential polarization range, an overall four-electron reduction of O_2 to H_2O was found to be the dominating process. The kinetic parameters obtained from the RDE experiments indicate that in a neutral solution, the reduction rate at the step from H_2O_2 to H_2O is faster than that seen from O_2 to H_2O_2. Carbon particle-based air cathodes catalyzed by CoTMPP were fabricated for metal-air fuel cell application. The obtained non-noble catalyst content cathodes show considerably improved performance and stability.

Keywords: Cobalt tetramethoxyphenyl porphyrin (CoTMPP); Oxygen; Hydrogen peroxide; Electrocatalysts; Air cathode; Metal-air fuel cells

1. Introduction

As efficient, clean, energy converters, fuel cells have attracted much attention in recent years due to the possible energy crisis induced by increasing power demands and the increasing importance of protecting our environment. However at the current stage of technology, high cost is one of the big obstacles hindering the commercialization of fuel cells. Developing non-noble catalysts to replace expensive platinum-based catalysts is one of the major approaches being explored to reduce the cost [1–3]. Among the non-noble catalysts that have been discovered, metalloporphyrin complexes have been investigated for several decades as promising candidates for a fuel cell oxygen reduction reaction (ORR) catalyst [4–11]. A series of metalloporphyrin complexes were found to exhibit comparable activity and also higher tolerance to contamination in comparison with Pt-based electrocatalysts. However, most of the monomeric metalloporphyrins can only reduce oxygen to a stage of hydrogen peroxide through a two-electron pathway rather than a four-electron pathway to H_2O. The resulting hydrogen peroxide could corrode the catalyst and other cathode components, causing the degradation in catalyst activity and reduction in the lifetime of the cathode. In an effort to improve this process, a heat treatment was found to be an efficient way to improve four-electron catalyst activity, and catalyst stability [12–18].

In the past two to three decades, much work has been devoted to investigating the mechanism and kinetics of the metalloporphyrin-catalyzed ORR using cyclic voltammetric and rotating disk electrode techniques [19–29]. Most of this work has focused on the ORR with limited attention to the cat-

* Corresponding author. Tel.: +1 604 221 3087; fax: +1 604 221 3001.
** Corresponding author. Tel.: +1 604 940 3232.
E-mail addresses: jiujun.zhang@nrc.gc.ca (J. Zhang), jjung@dccnet.com (J. Jung).

0378-7753/$ – see front matter.
doi:10.1016/j.jpowsour.2006.04.132

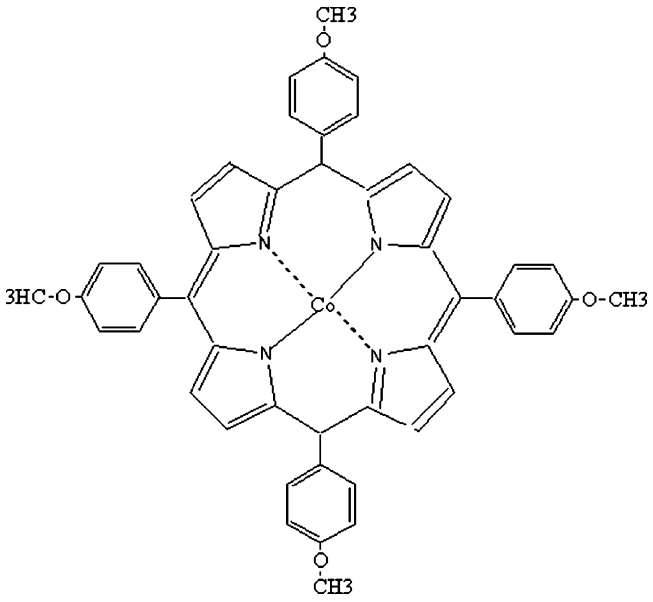

Fig. 1. The molecular structure of cobalt tetra-methoxy-phenyl porphyrin (CoTMPP).

alyzed hydrogen peroxide reduction. If the catalyst has activity towards H_2O_2 reduction, the produced H_2O_2 in the first ORR step ($O_2 + 2H^+ + 2e^- \Rightarrow H_2O_2$) could be eliminated to reduce its negative impact on the lifetime of the cathode and its performance. On the other hand, most previous works were carried out in strong acidic or alkaline solutions with emphasis on hydrogen-fueled fuel cell application. Limited attention has been put on neutral solutions, which are widely used in some metal-air fuel cells such as magnesium-air and aluminum-air fuel cells [30].

A typical metalloporphyrin, cobalt tetramethoxyphenyl porphyrin (CoTMPP, whose molecular structure is shown in Fig. 1), has been used as a catalyst in carbon particle-based air cathodes for application in the metal-air fuel cell [31,32]. In terms of fundamental understanding, more attention should be put on the exploration of the mechanism and kinetics of the CoTMPP catalytic process in the oxygen and hydrogen peroxide electroreduction. In this paper, cyclic voltammetry and the rotating disk electrode technique were used to study the surface behavior of adsorbed CoTMPP on a graphite electrode and its catalytic activity towards O_2 and H_2O_2 reduction. The ORR kinetic parameters were obtained and possible mechanisms were also proposed based on experimental observation and the literature. For practical application, the anion and temperature effects on the electrocatalytic behavior of CoTMPP were also studied. Some carbon particle-based air cathodes catalyzed by CoTMPP were fabricated to verify the catalytic effect in a practical neutral environment.

2. Experimental

2.1. Chemicals

CoTMPP was purchased from Sigma–Aldrich. Other chemicals such as H_2SO_4, NaOH, H_3PO_4, H_3BO_3, CH_3COOH, Na_2SO_4, NaCl, NaBr, NaF, ethanol, 5% Nafion solution, 60% polytetrafluoroethylene (PTFE) solution and 30% H_2O_2 aqueous solution were purchased from Sigma–Aldrich, and used without further purification. Double distilled water was further purified through an ultra-purification system (Millipore Water System), which was then used for the solution preparation. Britton–Robinson buffer solutions (abbreviated as BR buffer) ($CH_3COOH + H_3BO_3 + H_3PO_4 + NaOH$, 0.04 mol dm^{-3} for each component) were used to study the pH dependence. The pH adjustment was obtained by adding 1.0 M NaOH or 0.5 M H_2SO_4 to the intended electrolytes with BR buffer solution. Argon gas with high purity of 99.99% was used to bubble through the test solution to remove dissolved oxygen. In the oxygen reduction experiments, 99.99% air was used to saturate the test solution with a bubbling period of 10 min.

2.2. Electrode preparation

A rotating disk electrode was prepared by sealing pyrolytic graphite electrodes into the end of the copper shaft with heat shrinkable polyolefin tubing. The exposed active electrode area was 0.16 cm^2, which was calibrated electrochemically by a 1×10^{-3} mol dm^{-3} solution of $K_3[Fe(CN)_6]$. The electrode was polished using 0.5 μm alumina, sonicated for 5 min in water and rinsed with acetone and water before each experiment. To upload the catalyst, the polished electrode was dipped into a solution containing CoTMPP, which was prepared by dissolving 10 mg of CoTMPP in a mixture of deionized water (15 mL) and ethanol (15 mL). After soaking for a period of 30 s, the electrode was taken out and rinsed with water, then transferred to an electrochemical cell containing the intended electrolyte for measurement.

An air cathode with a two-layer structure was fabricated by using the rolling method. The gas diffusion layer (GDL) consisted of high-surface-area carbon particles and PTFE. The catalyst layer (CL) consisted of the carbon particles, CoTMPP, and PTFE. To distinguish the catalyst effect, another air cathode sample was prepared using a catalyst layer that contained the same weight of carbon particles and PTFE, but no CoTMPP. Metal mesh as the current collector was bonded between GDL and CL by a hot pressing process under a temperature of 330 °C and a pressure of 360 lb cm^{-2}.

2.3. Electrochemical measurements

Electrochemical measurements were performed in a custom-made three-compartment, three-electrode cell. A saturated calomel electrode (SCE) was used as the reference electrode, and a platinum wire as the auxiliary electrode. Cyclic voltammetry was conducted using a computerized SOLARTRON multichannel potentiostat. An ARS rotator (Pine Instruments) was employed for rotating disk voltammetry. Performance of the air cathode was tested by linear scan voltammetry in a custom-made half-cell. In this three-electrode half-cell, the working electrode mouth was designed to allow the GDL side to expose to the atmosphere and the CL side to contact with the electrolyte. The reference electrode was placed very closely to the CL surface. Due to the temperature dependence of SCE potential, all of the

potentials in the experiments that were involved in the temperature changes were calibrated to the reference level of SCE at 20 °C.

3. Results and discussion

3.1. Electrochemical behaviors of adsorbed CoTMPP

Fig. 2 shows the cyclic voltammograms (CVs) of adsorbed CoTMPP on a graphite electrode, recorded in 0.5 M H_2SO_4 and 1.0 M NaOH Ar-purged solutions, respectively. In acid solution, i.e., 0.5 M H_2SO_4 (Fig. 2(a), solid-line curve), three reversible redox waves (1/1′, 2/2′ and 3/3′, respectively) appear on the CV. The wave 1/1′ at the potential of 0.40 V should originate from the surface redox reaction of graphite electrode, which can be verified by the CV of the bare graphite electrode (dash-line curve). The wave 2/2′ near the potential of 0.54 V is relatively weak, which could be assigned to the cobalt center redox reaction. The wave 3/3′ near the potential of 0.78 V could be attributed to the N_4-ring redox reaction [33]. This wave has a half-peak width of 45 mV that can be expected, theoretically, for a two-electron reversible half-electrochemical reaction [34]. In the alkaline solution, i.e., 1.0 M NaOH (Fig. 2(b)), the CVs of adsorbed CoTMPP were also recorded. The redox wave from the graphite surface (wave 1/1′) is not visible in the studied potential range. In the potential range of −0.6 to +0.2 V (dot-line curve in Fig. 2(b)), the cobalt center redox wave (2/2′) appears near 0.03 V. When the potential is scanned to a more positive value such as +0.6 V, a large irreversible anodic wave appears near 0.50 V. Two processes may contribute to this wave. One is the N_4-ring oxidation, and the other is the oxygen evolution. After the irreversible oxidation of wave 3, the wave 2′ disappears, suggesting that the N_4-ring oxidation can damage the molecular structure of CoTMPP around the cobalt center, resulting in the irreversibility of cobalt center redox process. The detail of the oxidation mechanism of N_4-ring will not be pursued further in this paper.

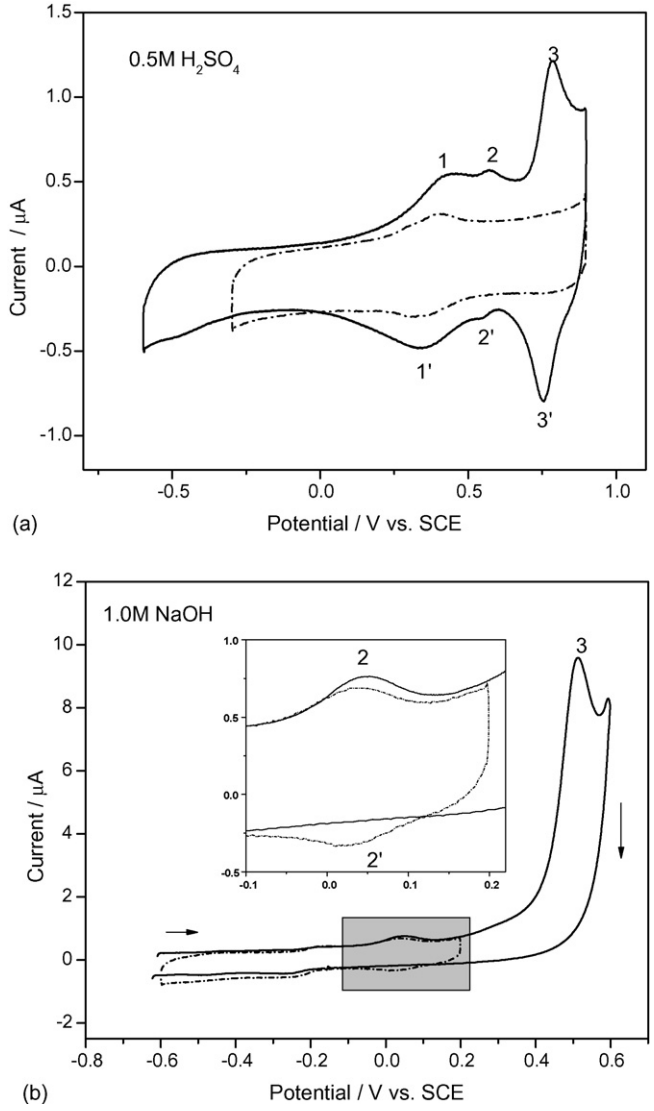

Fig. 2. Cyclic voltammograms (CVs) of adsorbed CoTMPP in (a) 0.5 M H_2SO_4 and (b) 1.0 M NaOH aqueous solutions. In (a), the dash-line CV represents the bare graphite electrode and the solid-line CV represents the CoTMPP-adsorbed graphite electrode. In (b), the dash-line CV is scanned between +0.2 and −0.6 V, while the solid-line CV is scanned between +0.6 and −0.6 V. Potential scan rate: 50 mV s^{-1}.

Surface CVs were also recorded at different potential scan rates for waves 2/2′ and 3/3′ in a 0.5 M H_2SO_4 solution. The average wave peak currents (I_p) were plotted as a function of potential scan rate, as shown in Fig. 3. For both waves, the linear relationships can be observed, and are a typical feature of a reversible redox surface reaction of an adsorbed species [34]. The theoretical expression for the linear relationship shown in Fig. 3 can be given as Eq. (1):

$$I_p = \left(\frac{n^2F^2}{4RT}\right) A\nu\Gamma_{\mathrm{CoTMPP}} \quad (1)$$

where n is the electron transfer number involved in the electrochemical reaction, F the Faraday constant, R the gas constant, T the temperature, A the electrode area, ν the potential scan

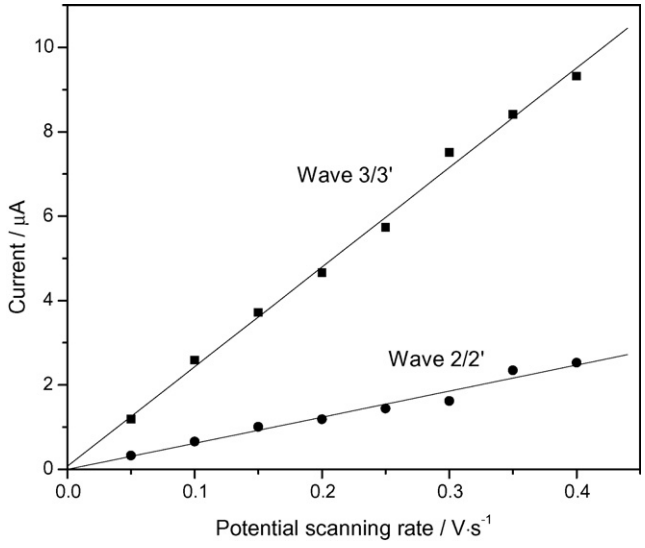

Fig. 3. The average peak currents of waves 2/2′ and 3/3′ as a function of the potential scan rate.

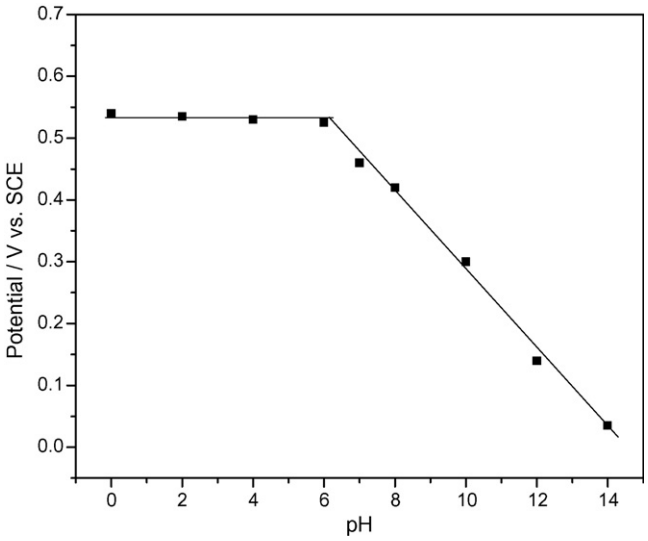

Fig. 4. The pH dependence of the formal potential of the cobalt redox reaction (wave 2/2′).

rate, and Γ_{CoTMPP} is the surface concentration of adsorbed CoTMPP. From the slope of I_p versus ν, either the surface concentration or the electron transfer number can be obtained. According to the slope of I_p versus ν plot of the wave 3/3′ for N_4-ring oxidation, the surface concentration was calculated to be 3.8×10^{-11} mol cm^{-2} with the assumption that this reaction is a two-electron process, as argued by the 45 mV of half-peak width. The electron number involved in the wave 2/2′ was then calculated to be 0.95, which is consistent with the assignment of one-electron reaction of Co^{II}/Co^{III} center.

In order to further explore the mechanism of the surface cobalt redox reaction, the pH dependence of the wave formal potential was obtained at various solution pHs, as shown in Fig. 4. The wave formal potential is taken as the average value of the anodic and the cathodic wave potentials. There are two distinct ranges with respect to pH. For a pH less than 6, the formal potential is independent of the pH, suggesting that the proton is not involved in the surface reaction at this pH range. When the pH is higher than 6, some pH dependent formal potentials can be observed with a slope of 63 mV pH^{-1}, which is very close to the theoretical value of 59 mV pH^{-1} for a reversible half-reaction involving one electron and one proton at 25 °C [34]. Thus the cobalt redox reaction mechanism of surface adsorbed CoTMPP can be written as reactions (2) and (3):

$$\mathrm{TMPP\text{-}Co^{III} + e^- \Leftrightarrow\ TMPP\text{-}Co^{II}} \quad (2)$$

$$\mathrm{TMPP\text{-}Co^{III} - OH^- + H^+ + e^- \Leftrightarrow\ TMPP\text{-}Co^{II} + H_2O} \quad (3)$$

Reaction (2) is predominant at pHs ≤ 6, while reaction (3) occurs at pHs > 6. This mechanism of surface cobalt redox reaction is similar to that of other cobalt porphyrins reported previously by Durand and Anson [19].

3.2. Surface adsorption orientation

The obtained surface concentration can give information about the surface adsorption orientation of CoTMPP molecules

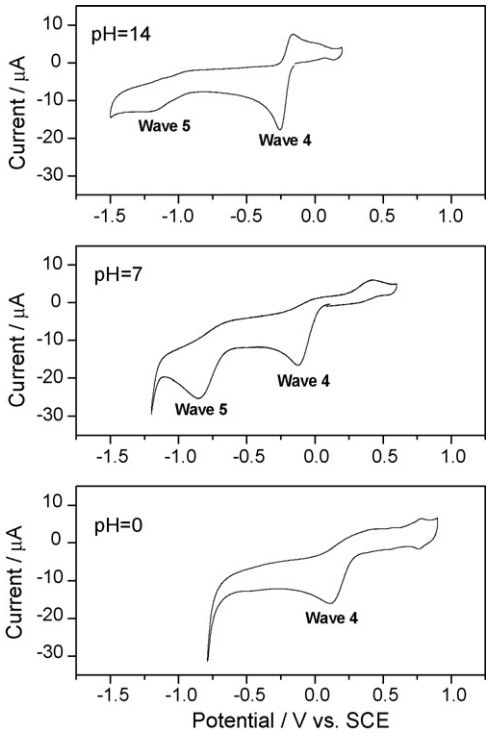

Fig. 5. Cyclic voltammograms of O_2 reduction on a CoTMPP adsorbed graphite electrode in an air saturated solution with three different pHs. Potential scan rate: 50 mV s^{-1}.

on the graphite electrode. According to the individual bond lengths [35], the molecular planar area of CoTMPP is about 5.1 nm^2. Thus, one monolayer adsorption of CoTMPP on the studied graphite electrode should give a theoretical surface concentration of 3.3×10^{-11} mol cm^{-2}, which is close to the measured value of 3.8×10^{-11} mol cm^{-2}, suggesting that all the molecules of CoTMPP have a flat orientation on the electrode surface.

3.3. Electrocatalytic activity of adsorbed CoTMPP towards O_2 and H_2O_2 reduction

Fig. 5 shows the cyclic voltammograms of oxygen reduction catalyzed by adsorbed CoTMPP on a graphite electrode in three air-saturated solutions with pH values of 14, 7 and 0, respectively. Different potential ranges were selected to focus on the oxygen and hydrogen peroxide reduction reaction. In a pH 14 solution, the onset potential for oxygen reduction (wave 4) is near −0.15 V which is 0.28 V away from the onset potential (∼0.13 V in Fig. 2(b)) of the cobalt center cathodic wave of adsorbed CoTMPP. At −1.16 V, a small bump (wave 5) is observed, which can be attributed to the further reduction of produced H_2O_2 in the first step of O_2 reduction (wave 4). Compared to the magnitude of wave 4, wave 5 is much smaller. This could be interpreted as the slow catalytic activity of CoTMPP towards H_2O_2 reduction or a direct four-electron reduction to water is occurring in parallel with the wave 4 in such an alkaline solution. In a rotating ring (Pt) – disk (carbon) electrode measurement to collect H_2O_2 produced during wave 4, it observed that the dominating product in wave 4 is H_2O_2. In a pH 7 solu-

tion, the first step of O_2 reduction (wave 4) appears near 0.05 V, followed by an equal magnitude of wave 5 for H_2O_2 reduction at ~0.65 V (Fig. 5(b)). The fact that the wave area of hydrogen peroxide reduction (wave 5) is almost equal to that of oxygen reduction (wave 4) may suggest that the produced H_2O_2 could all be reduced to water. At pH 0, the oxygen reduction wave onset potential moved to 0.29 V. It is impossible to record wave 5 for H_2O_2 reduction due to the early H_2 evolution reaction near −0.60 V in such an acidic solution. It is noteworthy that analogous experiments were carried out on the bare graphite electrode for comparison. Although some O_2 reduction currents were observed, the onset potentials on the bare electrode were more negative than those on a CoTMPP adsorbed electrode. This observation clearly confirms the catalytic effect of adsorbed CoTMPP.

It is commonly assumed that the oxygen reduction mechanism that is catalyzed by a metalloporphyrin occurs through an inner-sphere mechanism involved by the central metal redox center and the substrate [7,22,28]. The above results show that the oxygen reduction onset potential is well separated from cobalt redox potential regardless of the pH values. It may suggest that the bond between the CoTMPP cobalt center and O_2 or H_2O_2 in the adduct is too week so that the electron transfer from the substrate to the catalyst center becomes difficult. This result was also observed in other cobalt porphyrin catalyzed O_2 reduction mechanisms [18].

The pH dependence of the half-wave potential for catalyzed oxygen and hydrogen peroxide reduction was also investigated, as shown in Fig. 6. At a pH < 7, the half-wave potential of oxygen reduction decreases linearly with an increase in pH values with a slope of −49 mV pH^{-1}. At pH > 7, a pH independent feature can be observed. It suggests that the two-electron oxygen reduction reaction should involve two protons at a pH < 7, and when the pH > 7, the reduction reaction may not involve a proton or hydroxide ion change. For the subsequent H_2O_2 reduction, a linear relationship between the half-wave potential and pH with a slope of −57 mV pH^{-1} was observed, as in Fig. 6 in the pH range of 7–14. This slope may suggest that the two-electron reduction reaction of hydrogen peroxide involved two protons. At a pH < 6, the overlap of the hydrogen evolution wave with the wave of hydrogen peroxide reduction made it difficult to get the formal potential pH dependence.

Based on the above observations and the literature [19], the reaction sequence of the oxygen and subsequent hydrogen peroxide electro-reduction catalyzed by CoTMPP could be suggested as reactions (4)–(9):

In acidic solutions:

$$\text{TMPP-Co}^{\text{II}} + O_2 \Leftrightarrow \text{TMPP-Co}^{\text{II}} - O_2 \quad (4)$$

$$\text{TMPP-Co}^{\text{II}} - O_2 + 2H^+ + 2e^- \Leftrightarrow \text{TMPP-Co}^{\text{II}} + H_2O_2 \text{ (wave 4)} \quad (5)$$

In neutral or alkaline solutions:

$$\text{TMPP-Co}^{\text{II}} + OH^- + O_2 \Leftrightarrow \text{TMPP-Co}^{\text{II}} - O_2 + OH^- \quad (6)$$

$$\text{TMPP-Co}^{\text{II}} - O_2 + H_2O + 2e^- \Leftrightarrow \text{TMPP-Co}^{\text{II}} - OH^- + HO_2{}^- \text{ (wave 4)} \quad (7)$$

$$\text{TMPP-Co}^{\text{II}} - OH^- + HO_2{}^- \Leftrightarrow \text{TMPP-Co}^{\text{II}} - HO_2{}^- + OH^- \quad (8)$$

$$\text{TMPP-Co}^{\text{II}} - HO_2{}^- + H_2O + 2e^- \Leftrightarrow \text{(TMPP)Co}^{\text{II}} - OH^- + 2OH^- \text{ (wave 5)} \quad (9)$$

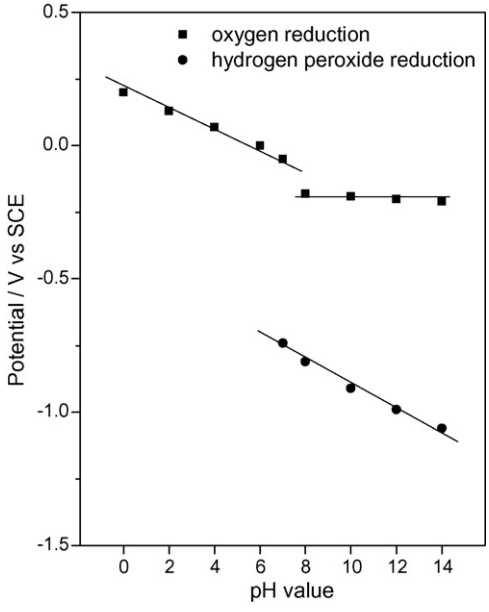

Fig. 6. The pH dependences of the half-wave potential of oxygen reduction and hydrogen peroxide reduction reactions on a graphite electrode adsorbed by CoTMPP.

3.4. Kinetics of oxygen and hydrogen peroxide reduction on adsorbed CoTMPP

In order to study the kinetics of the electrocatalyzed oxygen reduction, the current–potential curves were recorded at different rotating rates using a rotating disk graphite electrode on which the CoTMPP was adsorbed in air-saturated solutions with different pH values. Fig. 7(a) shows a typical example of current-potential curves obtained in an air-saturated pH 7 solution. Two stages of limiting current can be observed when the potential is scanned from OCV to −1.3 V, indicating that the electrocatalytic reduction of oxygen could be controlled by the diffusion process. In addition, the plateau current at the second stage can be seen to be nearly twice of that of the first stage, suggesting that if the oxygen reduction in the first stage is a two-electron process, the oxygen reduction at the second stage should be an overall four-electron process from oxygen to water in the neutral solution.

In Fig. 7(b), the reciprocals of the plateau currents at −0.6 and −1.2 V (taken from Fig. 7(a)) were plotted respectively against the reciprocals of the square root of the rotating rate. For comparison, two dot-lines calculated by the Koutecky–Levich theory, according to two- and four-electron oxygen reduction processes,

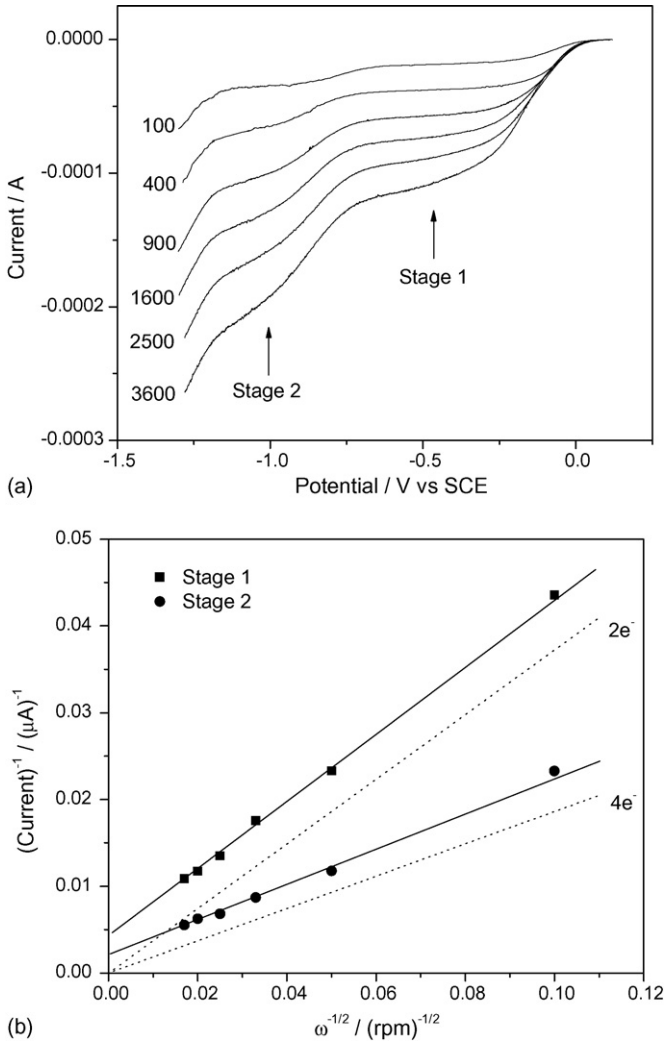

Fig. 7. (a) The current–potential curves at various rotating rates for oxygen reduction on a graphite rotating disk electrode with adsorbed CoTMPP. Potential scan rate: 10 mV s^{-1}; (b) Koutechy–Levich plots of the current–rotating rate data from (a).

were also plotted in the figure [36]. The experimental line at the first stage is close to being parallel to the calculated two-electron line, suggesting that the O_2 reduction is a two-electron process. For the oxygen reduction at the second stage, the measured line is parallel to that calculated for the four-electron process, indicating that the overall process of oxygen reduction is a four-electron reaction to produce water. It is believed that this four-electron process is consisted of two successive two-electron processes.

The plots in Fig. 7(b) can be interpreted on the basis of the Koutecky–Levich equation [36]:

$$\frac{1}{I_{\text{lim}}} = \frac{1}{I_{\text{lev}}} + \frac{1}{I_{\text{k}}} \tag{10}$$

where I_{lim} is the measured limiting current. I_{lev} and I_{k} are the Levich diffusion current and the kinetic current defined by Eqs. (11) and (12), respectively:

$$I_{\text{lev}} = 0.201nFAC_{O_2}D_{O_2}^{2/3}\gamma^{-1/6}\omega^{1/2} \tag{11}$$

$$I_{\text{k}} = nFAK_{O_2}C_{O_2}\Gamma_{\text{CoTMPP}} \tag{12}$$

Table 1
Kinetic currents and rate constants of oxygen reduction at pH 0, 7 and 14

pH	I_{k} at −0.6 V (μA)	K_{O_2} (mol^{-1} cm^3 s^{-1})
0	201	7.0×10^8
7	193	6.7×10^8
14	175	6.1×10^8

where n, D_{O_2}, and C_{O_2} are the overall electron number, the diffusion coefficient and oxygen concentration, respectively, γ the kinetic viscosity of the electrolyte solution (0.01 cm s^{-1}), ω the electrode rotating rate, and K_{O_2} is the rate constant of the chemical reaction which limits the plateau current. Due to that the currents were taken at the electrode potential ranges where the plateau currents occurred, the K_{O_2} obtained through kinetic currents should be potential independent, suggesting that this constant is for a chemical reaction rather than an electrochemical reaction. The other terms in Eqs. (11) and (12) have their usual significance. I_{k} can be obtained experimentally from the Y-intercept of the Koutecky–Levich line in Fig. 7(b). The value of K_{O_2} can be calculated from I_{k} according to the Eq. (12) with n, C_{O_2}, and Γ_{CoTMPP} determined. Table 1 summarizes the kinetic current (I_{k}) and the rate constant (K_{O_2}) calculated by the plateau current data at −0.6 V, which is corresponding to the process of oxygen reduced to hydrogen peroxide in the pH 0, 7, and 14 solutions. The obtained rate constant values are very close, suggesting that the pH has very little effect on the kinetics of catalyzed oxygen reduction at the first stage.

To investigate the kinetics of hydrogen peroxide reduction, analogous experiments were carried out in Ar-purged solutions containing 0.28 mM H_2O_2 with pH of 7 and 14, respectively. The reaction mechanism proposed by reactions (8) and (9) can be used to describe the reduction process of H_2O_2.

Fig. 8(a) shows the current–potential curves of hydrogen peroxide reduction at different rotating rates in pH 7 solution. The currents at −1.3 V were measured to plot the Koutechky–Levich line, as shown in Fig. 8(b). The Y-Intercept of the Koutechky–Levich line was used to calculate the kinetic rate constants as listed in Table 2. The rate constant in the alkaline solution is seen to be much lower than that seen in the neutral solution. This result could be at least partially attributed to the strong adsorption in reaction (8). The OH^- in high concentration could compete with O_2 for available catalyst Co(II) centers, resulting in a slower O_2 reduction reaction. In addition, from Tables 1 and 2, the rate constant of hydrogen peroxide reduction in the neutral solution is seen to be higher than that of oxygen reduction, suggesting that CoTMPP can be used as a cathode catalyst for metal-air batteries or for fuel cells that are

Table 2
Kinetic currents and rate constants of hydrogen peroxide reduction at pH 7 and 14

pH	I_{k} at −1.3V (μA)	$K_{H_2O_2}$ (mol^{-1} cm^3 s^{-1})
7	345	1.2×10^9
14	72	2.5×10^8

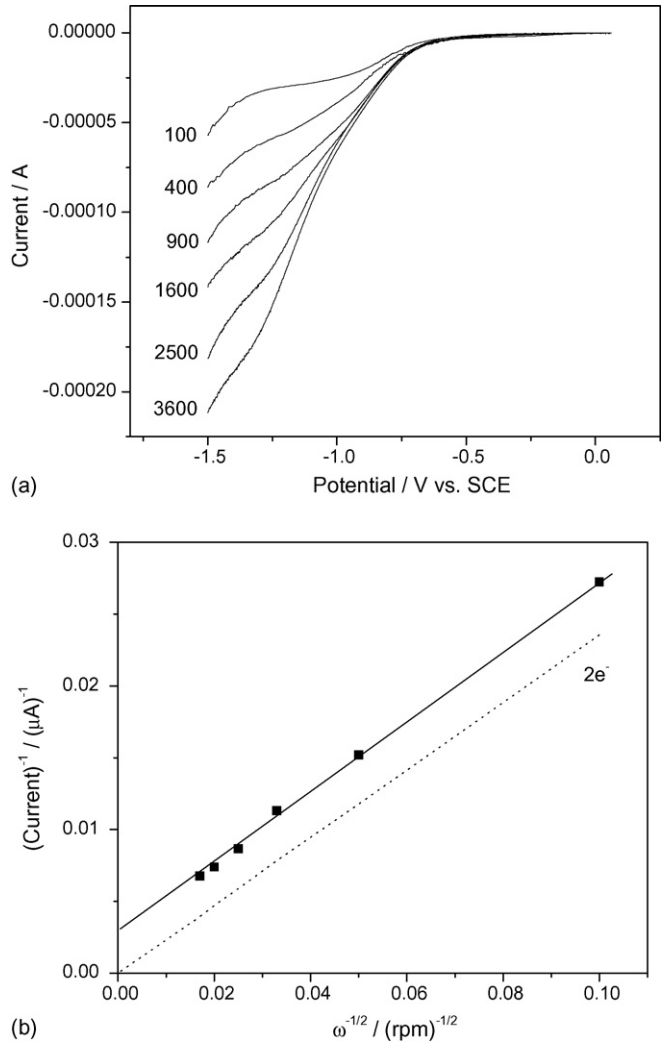

Fig. 8. (a) The current–potential curves at various rotating rates for hydrogen peroxide reduction on a graphite rotating disk electrode with adsorbed CoTMPP. Potential scan rate: 10 mV s^{-1}. (b) Koutechy–Levich plots of the current–rotating rate data from (a).

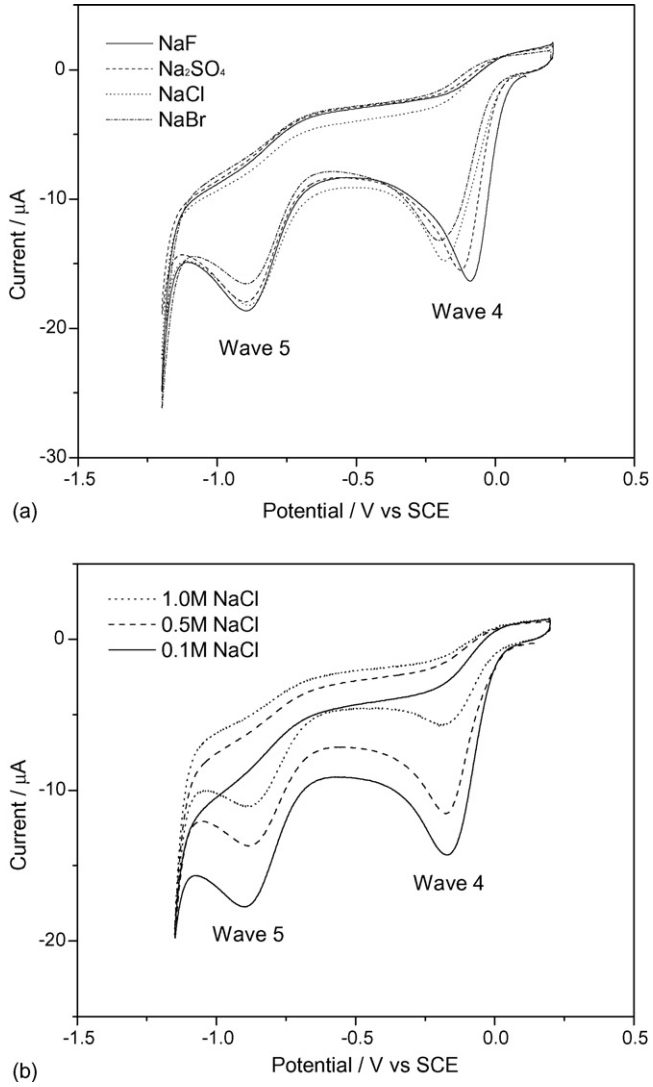

Fig. 9. (a) Cyclic voltammograms of adsorbed CoTMPP in 0.1 M air-saturated solutions with various anions; (b) cyclic voltammograms of adsorbed CoTMPP in NaCl air-saturated solutions with various concentrations. Potential scan rate: 50 mV s^{-1}.

operated in a neutral electrolyte to eliminate the accumulation of produced H_2O_2.

3.5. Effects of anion adsorption on electrocatalytic behaviors of adsorbed CoTMPP

The effect of anion adsorption on CoTMPP electrocatalytic behavior was investigated by adding a series of different anions into the electrolyte or using an electrolyte with different NaCl concentrations. Fig. 9(a) shows the cyclic voltammograms of O_2 reduction catalyzed by adsorbed CoTMPP in 0.1 M Na_2SO_4, NaF, NaCl and NaBr solutions. The solution pH was controlled at 7 by a BR buffer. The anion was found to have a significant effect on the onset potential of oxygen reduction. The onset potentials of oxygen reduction in NaF, Na_2SO_4, NaCl and NaBr solutions are 0.047, 0.027, 0.021 and 0.003 V, respectively. The potential shift may be attributed to the adsorption competition between the oxygen and anion on the catalyst sites. If the adsorption of an anion is stronger, oxygen will have difficulty replacing the anion on the catalyst sites in order to form CoTMPP-O_2 adducts, which results in a negative shift of the onset potential. The sequence of the onset potential for O_2 reduction is basically consistent with the order of adsorption ability of the anions on a mercury electrode, i.e., $Br^- > Cl^- > SO_4^{2-} > F^-$ [37], that is, the Br^- causes the largest potential shift and F^- has the smallest impact. A similar experiment to that depicted in Fig. 9(a) was also carried out to investigate the anion effect on H_2O_2 reduction. Basically, the anions have no influence on the onset potential of hydrogen peroxide reduction, suggesting that the adsorption ability of H_2O_2 may be strong enough to compete with other anions. On the other hand, the peak current of the oxygen reduction was also affected by the anions, suggesting that the anion can affect the kinetics of the reduction. For a quantitative explanation about the effects, more experiments and fundamental modeling are needed.

Fig. 9(b) shows the cyclic voltammograms of oxygen reduction on a CoTMPP adsorbed electrode in 0.1, 0.5 and 1.0 M NaCl solution with a pH value of 7. Both of the onset potentials of

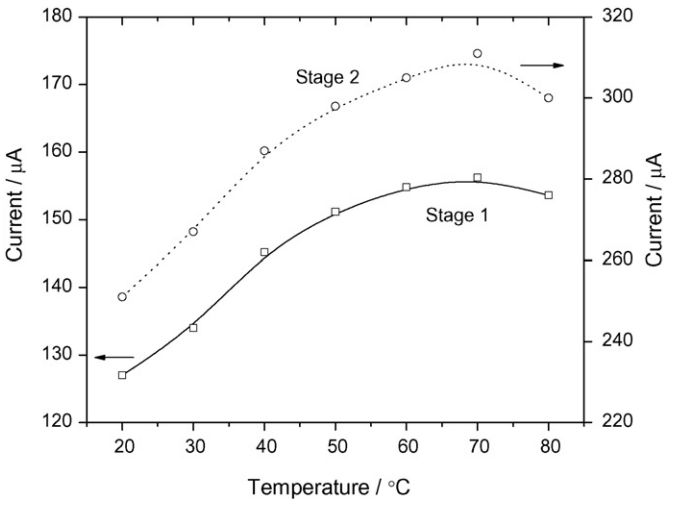

Fig. 10. Temperature dependences of the plateau current for oxygen reduction at two stages, at −0.6 and −1.2 V, respectively, on a graphite electrode adsorbed by CoTMPP in 0.1 M NaCl neutral solution.

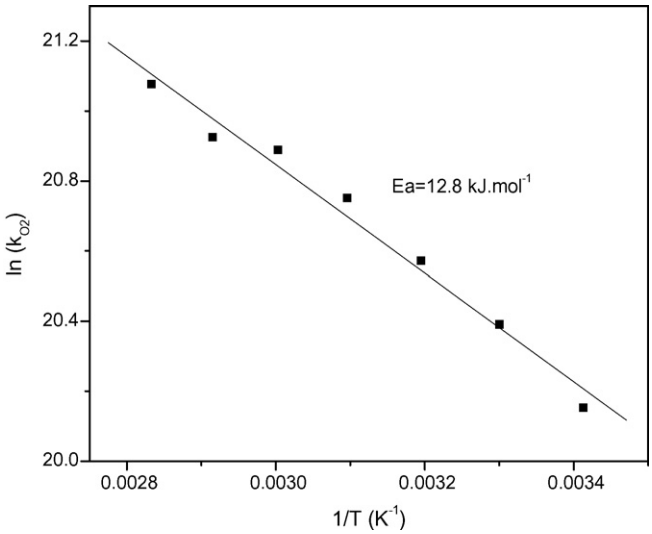

Fig. 11. An Arrehnius curve for the oxygen reduction electrocatalyzed by adsorbed CoTMPP on a graphite electrode in 0.1 M NaCl neutral solution.

oxygen reduction and hydrogen peroxide reduction were seen to be independent of the electrolyte concentrations, while the peak current was seen to decrease with an increase in NaCl concentration. This result indicates that the onset potential is not affected by the anion concentration. Only the kinetics, probably including both charge and mass transfers, is depressed by more concentrated NaCl solution.

3.6. Effects of temperature on the electrocatalytic behavior of adsorbed CoTMPP

The effect of temperature on oxygen reduction was also studied in a 0.1 M NaCl air-saturated solution (pH 7) at different temperatures using a rotating disk graphite electrode coated with CoTMPP. Fig. 10 shows the plateau currents of the first and second stages, at −0.6 and −1.2 V, respectively, as a function of temperature. With the increase in temperature from 20 to 70 °C, both plateau currents increase monotonically. Above 70 °C, a decrease in both plateau currents can be observed. Several factors can affect the plateau current, such as the oxygen concentration, viscosity, the diffusion coefficient, and the rate constants of oxygen reduction. These factors are also temperature dependent, as listed in Table 3 [35]. An increase in temperature causes decreases in the oxygen saturated concentration and viscosity, and an increase in the diffusion coefficient. The rate constants for oxygen reduction at different temperatures were calculated based on the plateau current data at −0.6 V and the parameters listed in Table 3 through the Koutecky–Levich theory.

The Arrehnius theory was also used to obtain the activation energy of the oxygen reduction reaction catalyzed by adsorbed CoTMPP. Based on the Arrehnius theory, the reaction rate constant can be expressed as a function of temperature:

$$\ln(K_{O_2}) = \ln({K_{O_2}}^0) - \frac{E_a}{RT} \quad (13)$$

where ${K_{O_2}}^0$ is the absolute reaction rate constant at $E_a = 0$ or T = infinite, E_a the activation energy for the reaction. Fig. 11 shows the plot of $\ln(K_{O_2})$ versus $1/T$, from which E_a can be estimated. In this case, E_a was calculated to be 12.8 kJ mol^{-1}.

3.7. Carbon particle-based air cathodes catalyzed by CoTMPP

As mentioned previously, CoTMPP has been used as a cathode catalyst for air cathodes in an effort to reduce cost especially in neutral and/or alkaline electrolyte-based, metal-air batteries and fuel cells [31,32]. In a joint project between the NRC Institute for Fuel Cell Innovation and MagPower System Inc., carbon particle-based air cathodes catalyzed by CoTMPP have been

Table 3
The effect of temperature on oxygen concentration, viscosity, diffusion coefficient and the rate constants of catalyzed oxygen reduction on a CoTMPP adsorbed graphite electrode

	Temperature (°C)						
	20	30	40	50	60	70	80
C_{O_2} (mol cm^{-3})[a]	0.28	0.22	0.19	0.17	0.15	0.13	0.10
γ (cm s^{-1})[a]	0.0100	0.0082	0.0065	0.0055	0.0047	0.0029	0.0016
D_{O_2} (cm^2 s^{-1})[a]	2.0×10^{-5}	2.4×10^{-5}	3.2×10^{-5}	4.0×10^{-5}	4.8×10^{-5}	5.5×10^{-5}	6.3×10^{-5}
K_{O_2} (mol^{-1} cm^3 s^{-1})	5.7×10^8	7.2×10^8	8.6×10^8	1.0×10^9	1.1×10^9	1.2×10^9	1.4×10^9

[a] Ref. [35].

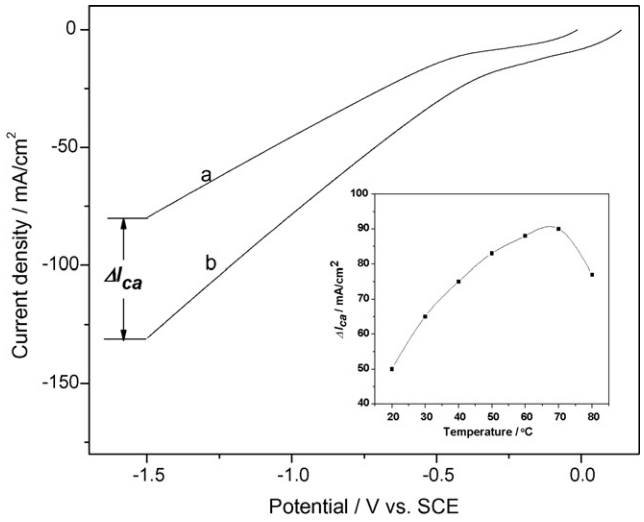

Fig. 12. Linear scan voltammograms of carbon particle-based air cathodes in a 10% NaCl solution. (a) Without CoTMPP catalyst in the catalyst layer; (b) with CoTMPP catalyst in the catalyst layer. Potential scan rate: 10 mV s^{-1}. The inset plot is the temperature dependence of catalytic current density ΔI_{ca}.

developed. Fig. 12 shows linear scan voltammograms of carbon particle-based air cathodes with and without CoTMPP catalyst in a 10% NaCl solution (pH ∼ 7). Compared to that of the bare carbon particle-based air cathode, the CoTMPP-catalyzed air cathode shows a higher open circuit electrode potential (OCEP) (0.13 V versus −0.02 V), indicating that the oxygen reduction will be easier on a CoTMPP catalyzed cathode than that on a bare cathode. With polarization from OCEP to −1.50 V, a current difference (ΔI_{ca}) can be observed, which should be attributed to the catalytic effect. As discussed in Fig. 5(b), in this potential range there are two successive reduction processes. In the potential range of 0.13V to −0.50 V, the dominating reaction is a two-electron reduction of oxygen producing H_2O_2; and in the potential range of −0.5 to −1.5 V, an overall four-electron process from O_2 to H_2O will occur. The temperature dependence of ΔI_{ca} was also investigated in the temperature range of 20–80 °C, as shown in the inset plot of Fig. 12. The catalytic current density increases with an increase in temperature up to 70 °C, and then decreases after the temperature reaches more than 70 °C. This tendency is consistent with the temperature dependence of plateau currents in Fig. 10. Thus, these results confirm that CoTMPP has a significant catalytic effect on the carbon particle-based air cathodes.

4. Conclusions

Surface electrochemical behavior of adsorbed CoTMPP on a graphite electrode was investigated at different solution pHs. Two surface waves were identified, one corresponds to the cobalt center one-electron redox process, and the other is the N_4-ring two-electron redox process. The adsorbed CoTMPP displays strong catalytic activity towards both oxygen and hydrogen peroxide reductions. The cobalt center is believed to be the catalytic active center, which may bond with O_2 or H_2O_2 to form an adduct that then helps the electron transfer from O_2 or H_2O_2 to the electrode, completing the reduction cycle. In acidic solutions, oxygen can only be reduced to the stage of hydrogen peroxide by a two-electron process. In neutral or alkaline solutions, oxygen is reduced to hydrogen peroxide in the low polarization potential range. With increasing potential polarization, the reduction becomes an overall four-electron process producing water. Anion adsorption and temperature show significant effects on the electrocatalytic behavior of adsorbed CoTMPP in a pH 7 neutral solution. The catalytic activity towards hydrogen peroxide reduction promotes CoTMPP as a feasible catalyst for the applications in some neutral electrolyte based metal-air batteries or fuel cells.

Acknowledgements

This work has been financially supported jointly by NRCs Institute for Fuel Cell Innovation and MagPower Systems Inc.

References

[1] W. Vielstich, A. Lamm, H. Gasteiger, Handbook of Fuel Cells – Fundamentals Technology and Applications, NJ, USA, Part 3, vol. 3–4, 2003.
[2] B. Wang, J. Power Sources 152 (2005) 1.
[3] L. Zhang, J.J. Zhang, D.P. Wilkinson, H.J. Wang, J. Power Sources 156 (2006) 171–182.
[4] R. Jasinski, Nature 201 (1964) 1212.
[5] J.P. Collman, P. Denisevich, Y. Konai, M. Marrocco, C. Koval, F. Anson, J. Am. Chem. Soc. 102 (1980) 6027.
[6] E. Yeager, J. Mol. Catal. 38 (1986) 5.
[7] K. Wiesener, D. Ohms, V. Neumann, R. Franke, Mater. Chem. Phys. 22 (1989) 457–475.
[8] P. Vasudevan, Santosh, N. Mann, S. Tyagi, Trans. Met. Chem. 15 (1990) 81.
[9] J. Collman, P. Wagenknecht, J. Hutchison, Angew. Chem. Int. Ed. Engl. 33 (1994) 1537.
[10] A. Biloul, P. Gouerec, M. Savy, G. Scarbeck, J. Appl. Electrochem. 26 (1996) 1139.
[11] A. Solovieva, S. Timashev, Russ. Chem. Rev. 72 (2003) 965.
[12] H. Jahnke, M. Schonbron, G. Zimmerman, Top. Curr. Chem. 61 (1976) 133.
[13] M. Ladouceur, G. Ladande, D. Guay, J.P. Dodelet, J. Electrochem. Soc. 140 (7) (1993) 1974.
[14] G.Q. Sun, J.T. Wang, R.F. Savinell, J. Appl. Electrochem. 28 (1998) 1087.
[15] S. Gojkovic, S. Gupta, R. Savinell, J. Electroanal. Chem. 462 (1999) 63.
[16] M. Lefevre, J. Dodelet, P. Bertrand, J. Phys. Chem. B 106 (2002) 8705.
[17] M. Tarasevich, K. Radyushkina, G. Zhutaeva, Russ. J. Electrochem. 40 (2004) 1369.
[18] A. Sirk, S. Campbell, V. Birss, Electrochem. Solid-State Lett. 8 (2005) 104.
[19] R. Durand, F. Anson, J. Electroanl. Chem. 134 (1982) 273.
[20] A. Putten, A. Elzing, W. Visscher, E. Barendrecht, J. Electroanal. Chem. 221 (1987) 95.
[21] C. Kang, Y. Xie, F. Anson, J. Electroanal. Chem. 413 (1996) 165.
[22] J. Zhang, Y. Tse, W. Pietro, A. Lever, J. Electroanal. Chem. 406 (1996) 203.
[23] C. Shi, B. Steiger, M. Yuasa, F. Anson, Inorg. Chem. 36 (1997) 4294.
[24] E. Song, C. Shi, F. Anson, Langmuir 14 (1998) 4315.
[25] T. Chung, F. Anson, J. Electroanal. Chem. 508 (2001) 115.
[26] G. Zhutaeva, G. Boikova, K. Radyushkina, M. Tarasevich, Russ. J. Electrochem. 38 (2002) 1229.
[27] K. Kadish, L. Fremond, Z. Ou, J. Shao, C. Shi, F. Anson, F. Burdet, C. Gros, J. Barbe, R. Guilard, J. Am. Chem. Soc. 127 (2005) 5625.

[28] L. Zhang, C. Song, J. Zhang, H. Wang, D. Wilkinson, J. Electrochem. Soc. 152 (2005) A2421.
[29] C. Song, L. Zhang, J. Zhang, H. Wang, D. Wilkinson, 3rd European PEFC Forum, 4–8, July 2005, Lucerne, Switzerland.
[30] D. Linden, T.B. Reddy, Handbook of Batteries, McGraw-Hill, New York, 2002.
[31] S. Sathyanarayana, N. Munichandraiah, J. Appl. Electrochem. 11 (1981) 33.
[32] M. Maja, C. Orecchia, M. Strano, P. Tosco, M. Vanni, Electrochim. Acta 46 (2000) 423.
[33] E. Barefield, F. Lovecchio, N. Tokel, E. Ochiai, D. Busch, Inorg. Chem. 11 (1972) 283.
[34] A. Bard, L. Faulkner, Electrochemical Methods, "Fundamentals and Applications", Wiley, New York, 1980.
[35] B. Wolf, CRC Handbook of Chemistry and Physics, 85th ed., CRC Press, 2004–2005.
[36] J. Koutecky, V. Levich, Zh. Fiz. Khim. 32 (1958) 1565.
[37] C. Cha, Kinetics of Electrode Process, Science Press of China, Beijing, 2002.